


MEMORY REDUCTION USING A RING ABSTRACTION OVER GPU RDMA FOR DISTRIBUTED QUANTUM MONTE CARLO SOLVER

A PREPRINT

Weile Wei 
Louisiana State University
wwei9@lsu.edu

Eduardo D’Azevedo 
Oak Ridge National Laboratory
dazevedoef@ornl.gov

Kevin Huck 
University of Oregon
khuck@cs.uoregon.edu

Arghya Chatterjee ^{*}
NERSC, Berkeley Lab
ronnie@lbl.gov

Oscar Hernandez 
Oak Ridge National Laboratory
oscar@ornl.gov

Hartmut Kaiser 
Louisiana State University
hkaiser@cct.lsu.edu

May 14, 2021

ABSTRACT

Scientific applications that run on leadership computing facilities often face the challenge of being unable to fit leading science cases onto accelerator devices due to memory constraints (memory-bound applications). In this work, the authors studied one such US Department of Energy mission-critical condensed matter physics application, Dynamical Cluster Approximation (DCA++), and this paper discusses how device memory-bound challenges were successfully reduced by proposing an effective “all-to-all” communication method—a ring communication algorithm. This implementation takes advantage of acceleration on GPUs and remote direct memory access (RDMA) for fast data exchange between GPUs.

Additionally, the ring algorithm was optimized with sub-ring communicators and multi-threaded support to further reduce communication overhead and expose more concurrency, respectively. The computation and communication were also analyzed by using the Autonomic Performance Environment for Exascale (APEX) profiling tool, and this paper further discusses the performance trade-off for the ring algorithm implementation. The memory analysis on the ring algorithm shows that the allocation size for the authors’ most memory-intensive data structure per GPU is now reduced to $1/p$ of the original size, where p is the number of GPUs in the ring communicator. The communication analysis suggests that the distributed Quantum Monte Carlo execution time grows linearly as sub-ring size increases, and the cost of messages passing through the network interface connector could be a limiting factor.

Keywords DCA++, Quantum Monte Carlo, GPU Remote Direct Memory Access, memory-bound issue, exascale machines

1 Introduction

Dynamical Cluster Approximation (DCA++)² is a high-performance research software application [1, 2, 3, 4] that provides a modern C++ implementation to solve quantum many-body problems. DCA++ implements a quantum cluster method with a Quantum Monte Carlo (QMC) kernel for modeling strongly correlated electron systems. The DCA++ software currently uses three different programming models—message passing interface (MPI), Compute Unified Device Architecture (CUDA), and High Performance ParalleX (HPX)/C++ threading—together with three

^{*}Arghya Chatterjee contributed to this work mostly during his previous appointment at Oak Ridge National Laboratory, Oak Ridge, TN.

²DCA++ is available at <https://github.com/CompFUSE/DCA>

numerical libraries—Basic Linear Algebra Subprograms (BLAS), Linear Algebra Package (LAPACK), and Matrix Algebra on GPU (MAGMA)—to expose the parallel computation.

In the QMC kernel [5], the two-particle Green’s function (G_t) is needed for computing important fundamental quantities, such as the critical temperature (T_c), for superconductivity. In other words, a larger G_t allows condensed matter physicists to explore larger and more complex (i.e., higher fidelity) physics cases. DCA++ currently stores G_t in a single GPU device. However, this limits the largest G_t that can be processed within one GPU. A new approach for partitioning the large G_t across the multiple GPUs can significantly increase scientists’ capabilities to explore higher fidelity simulations. This paper focuses on how the memory-bound issue in DCA++ was successfully addressed by proposing an effective “all-to-all” communication method—a ring algorithm—to update the distributed G_t device array.

1.1 Contributions

The primary contributions of this work are outlined as follows.

1. The memory consumption in a QMC solver application was reduced to store a much larger G_t array across multi-GPUs. This significant contribution enables physicists to evaluate larger scientific problem sizes and compute the full G_t array in a single computation, which significantly increases the accuracy/fidelity of the simulation of a certain material.
2. A ring abstraction layer was designed that updates the large distributed G_t array. The ring algorithm was further improved by adding sub-ring communicator and multi-threaded communication to reduce communication overhead and expose more concurrency, respectively.
3. The ring abstraction layer was implemented on top of NVIDIA GPUDirect remote direct memory access (RDMA) for fast device memory transfer.
4. The Autonomic Performance Environment for Exascale (APEX) performance measurement library was extended to support the use case, driving tool development and research.

2 Background

QMC solver applications are widely used and are mission-critical across the US Department of Energy’s (DOE’s) application landscape. For the purpose of this paper, the authors chose to use one of the primary QMC applications, the DCA++ code. A production-scale scientific problem runs on DOE’s fastest supercomputer, Summit, at the Oak Ridge Leadership Computing Facility on all 4,600 nodes; each node contains six NVIDIA Volta V100 GPUs, attaining a peak performance of 73.5 PFLOPS with a mixed precision implementation [5].

Monte Carlo simulations are embarrassingly parallel, and the authors exploited this on distributed systems with a two-level (MPI + threading) parallelization scheme (Figure 1). Although DCA++ has been highly optimized and is scalable on existing hardware, this is the first effort to focus on solving the memory-bound issue described in Section 1 and further take advantage of Summit’s GPU RDMA capability.

Figure 1 shows the parallelism hierarchy in one iteration of the QMC solver (MPI distribution + on-node threading parallelism). For example, each rank $\{R0, \dots, RN\}$ is assigned a Markov Chain and the initial input (two particle Green’s function, $G_{t,i}$, where t means “two-particle,” and i is rank index). Each rank spawns multiple independent worker threads (i.e., walkers and accumulators). Most work and computation are performed on the GPU. Each walker thread generates a measurement result ($G_{\sigma,i}$ array, where i is thread ID) by performing nonuniform Fourier transform implemented by matrix-matrix multiplication. Each walker passes its $G_{\sigma,i}$ to its corresponding accumulator thread. In other words, each thread has its own $G_{\sigma,i}$ array, and each rank will have k different $G_{\sigma,i}$ arrays, where k is the number of walker threads per rank. Each accumulator thread then updates $G_{t,i}$ via the formula in Eq. (1) to compute and update rank-local $G_{t,i}$ to $G'_{t,i}$. The updated partial $G'_{t,i}$ is then fed into the coarse-graining step for the next measurement. At the end of all measurements, an MPI_Reduce operation will be performed on G_t across all ranks to produce a final and complete G_t in the root rank. G_t is allocated before all measurements start and has a life that spans until the end of the DCA++ program.

2.1 Memory-Bound Issue in DCA++

The results from Balduzzi et al. [5] show that although storing a G_t on the accelerator device allows condensed matter scientists to explore larger and more complex (i.e., higher fidelity) physics cases, the problem size is limited to the device memory size. Updating the device array G_t is the most time-consuming and memory-intensive process

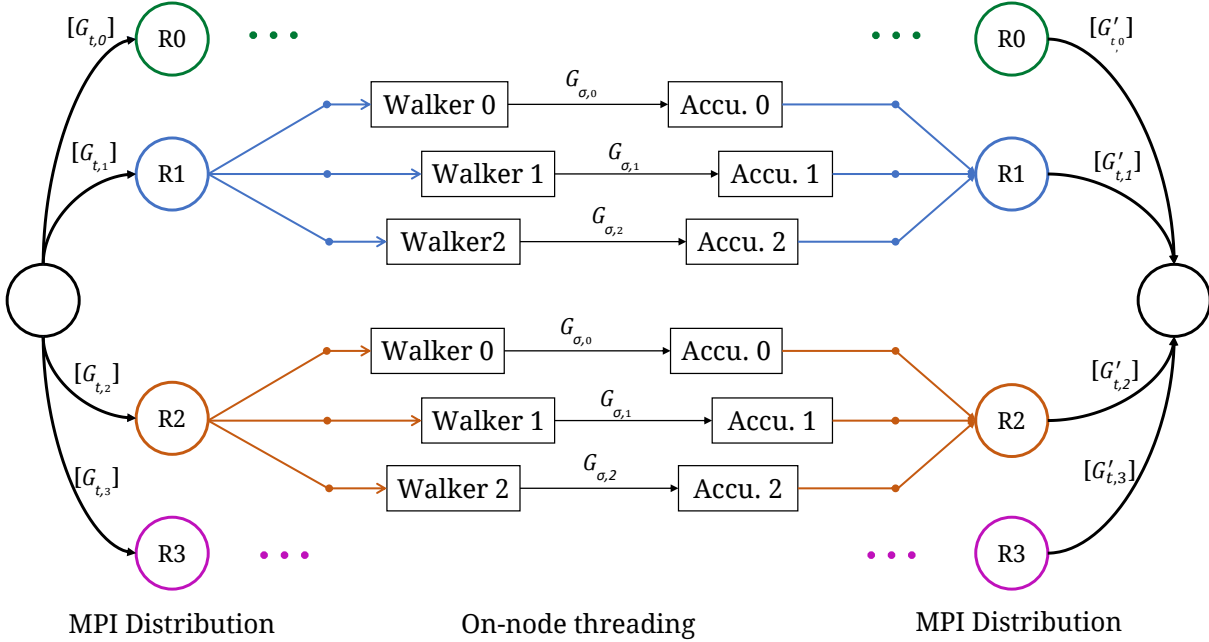


Figure 1: Workflow of the QMC DCA++ solver.

throughout DCA++ computation. A distributed G_t approach is needed to reduce memory allocation and operation in the device.

In the original DCA++ algorithm, G_t is updated by a product of two smaller matrices (single-particle Green's function, or G_σ). This computation update is in the particle-particle channel and is accumulated according to Eq. (1).

$$G_t(K_1, K_2, K_3) += \sum_{\sigma} G_{\sigma}(K_3 - K_2, K_3 - K_1) G_{-\sigma}(K_2, K_1), \quad (1)$$

where K_i is a combined index that represents a particular point in the momentum and frequency space, and $\sigma = +1$ or -1 specifies the electron spin value. G_σ is the single-particle Green's function that describes the configuration of single electrons.

The ability to handle a larger G_t allows simulations of complex materials to significantly increase the details, accuracy, and fidelity. In the previous design that kept G_t within one GPU, only a sub-slice of G_t could be computed in a single computation. For the simple single-orbital coarse-grained Hubbard model, physics insights or prior knowledge can be used to decide which sub-slices in G_t contain the important physics and thus avoid the generation of full G_t . This simple model allows the generic behavior that comes from electronic corrections in materials to be studied, but it cannot distinguish between different specific materials. Material-specific modeling requires more complex models that include more orbital—and other—degrees of freedom, and this requires a much larger G_t . This new distributed ring implementation enables the full large G_t array to be computed in a single computation, even for more complex multi-orbital models, to ensure that no important physics cases are overlooked.

2.2 GPU RDMA Technology

GPU RDMA allows direct peer access to multi-GPU memory through a high-speed network. For NVIDIA GPUs, GPUDirect is a technology that allows for the direct transfer of data in GPU device memory to other GPUs on the same node by using the NVLINK2 interconnect and/or between GPUs on different nodes by using RDMA support that can bypass buffers on host memory.

A CUDA-aware MPI³ implementation can directly pass the GPU buffer pointer to MPI calls. Acceleration support, such as GPUDirect, can be used by the MPI library and allows buffers being sent from the kernel memory to a network

³<https://developer.nvidia.com/blog/introduction-cuda-aware-mpi/>

without staging through host memory. There are various CUDA-aware MPI implementations, such as OpenMPI, MVAPICH2, and IBM Spectrum MPI⁴.

3 Implementation: Ring Abstraction

3.1 Distributed G_t in QMC Solver

Before introducing the communication phase of the ring abstraction layer, it is important to understand how the authors distributed the large device array G_t across MPI ranks. Original G_t was compared, and G_t^d versions were distributed (Figure 2).

In the original G_t implementation, the measurements—which were computed by matrix-matrix multiplication—are distributed statically and independently over the MPI ranks to avoid inter-node communications. Each MPI rank keeps its partial copy of $G_{t,i}$ to accumulate measurements within a rank, where i is the rank index. After all the measurements are finished, a reduction step is taken to accumulate $G_{t,i}$ across all MPI ranks into a final and complete G_t in the root MPI rank. The size of the $G_{t,i}$ in each rank is the same size as the final and complete G_t .

With the distributed G_t^d implementation, this large device array G_t was evenly partitioned across all MPI ranks; each portion of it is local to each MPI rank. Instead of keeping its partial copy of G_t , each rank now keeps an instance of $G_{t,i}^d$ to accumulate measurements of a portion or sub-slice of the final and complete G_t , where the notation d in G_t^d refers to the distributed version, and i means the i -th rank. The $G_{t,i}^d$ size in each rank is reduced to $1/p$ of the size of the final and complete G_t , comparing the same configuration in original G_t implementation, where p is the number of MPI ranks used. For example, in Figure 2b, there are four ranks, and rank i now only keeps $G_{t,i}^d$, which is one-fourth the size of the original G_t array size.

To compute the final and complete G_t^d for the distributed G_t^d implementation, each rank must see every $G_{\sigma,i}$ from all ranks. In other words, each rank must broadcast the locally generated $G_{\sigma,i}$ to the remainder of the other ranks at every measurement step. To efficiently perform this “all-to-all” broadcast, a ring abstraction layer was built (Section. 3.2), which circulates all $G_{\sigma,i}$ across all ranks.

3.2 Pipeline Ring Algorithm

A pipeline ring algorithm was implemented that broadcasts the G_σ array circularly during every measurement. The algorithm (Algorithm 1) is visualized in Figure 3.

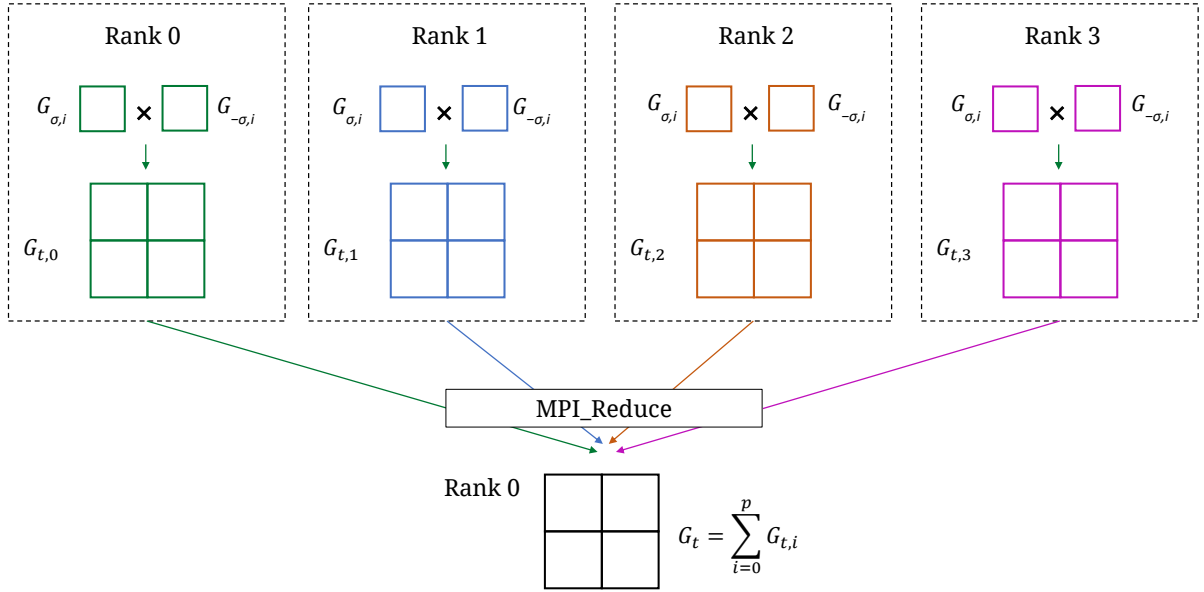
Algorithm 1: Pipeline ring algorithm

```

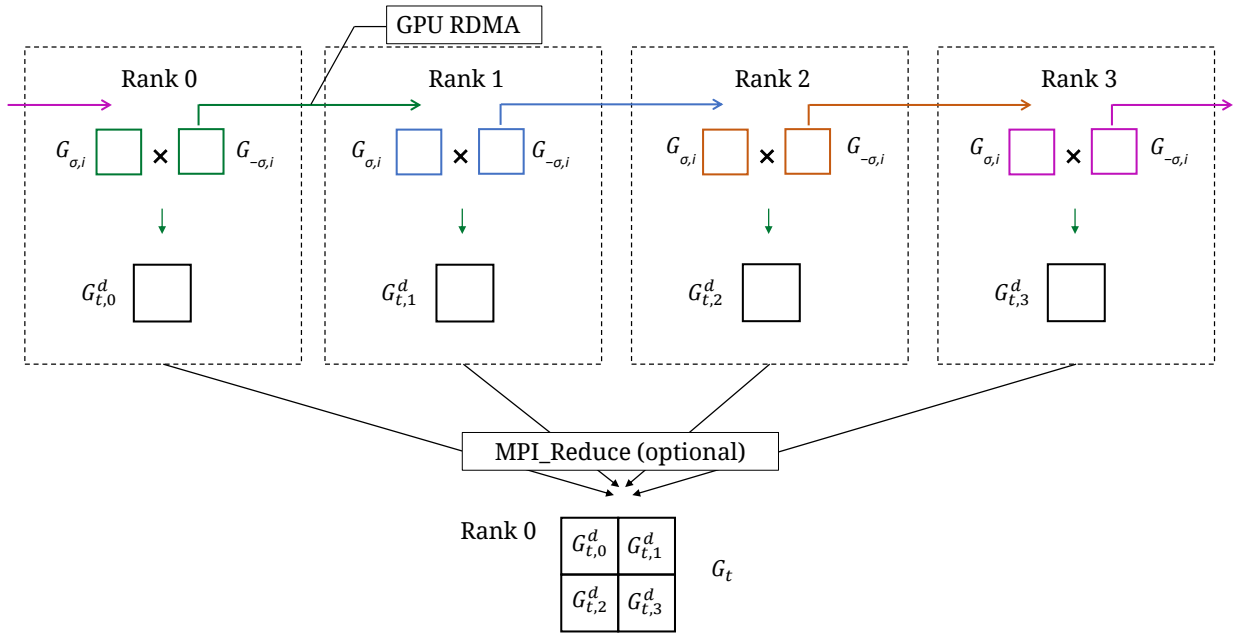
1 generateGSigma(gSigmaBuf);
2 updateG4(gSigmaBuf);
3  $i \leftarrow 0$ ;
4  $myRank \leftarrow worldRank$ ;
5  $ringSize \leftarrow mpiWorldSize$ ;
6  $leftRank \leftarrow (myRank - 1 + ringSize) \% ringSize$ ;
7  $rightRank \leftarrow (myRank + 1 + ringSize) \% ringSize$ ;
8  $sendBuf.swap(gSigmaBuf)$ ;
9 while  $i < ringSize$  do
10    $MPI\_Irecv(recvBuf, source=leftRank, tag = recvTag, recvRequest)$ ;
11    $MPI\_Isend(sendBuf, source=rightRank, tag = sendTag, sendRequest)$ ;
12    $MPI\_Wait(recvRequest)$ ;
13    $updateG4(recvBuf)$ ;
14    $MPI\_Wait(sendRequest)$ ;
15    $sendBuf.swap(recvBuf)$ ;
16    $i++$ ;
17 end

```

⁴IBM Spectrum MPI is supported on the Summit supercomputer, and is also the CUDA-aware MPI implementation used by the authors in this paper.



(a) Original G_t implementation.



(b) Distributed G_t implementation.

Figure 2: Comparison of the original G_t vs. the distributed G_t^d implementation. Each rank contains one GPU resource.

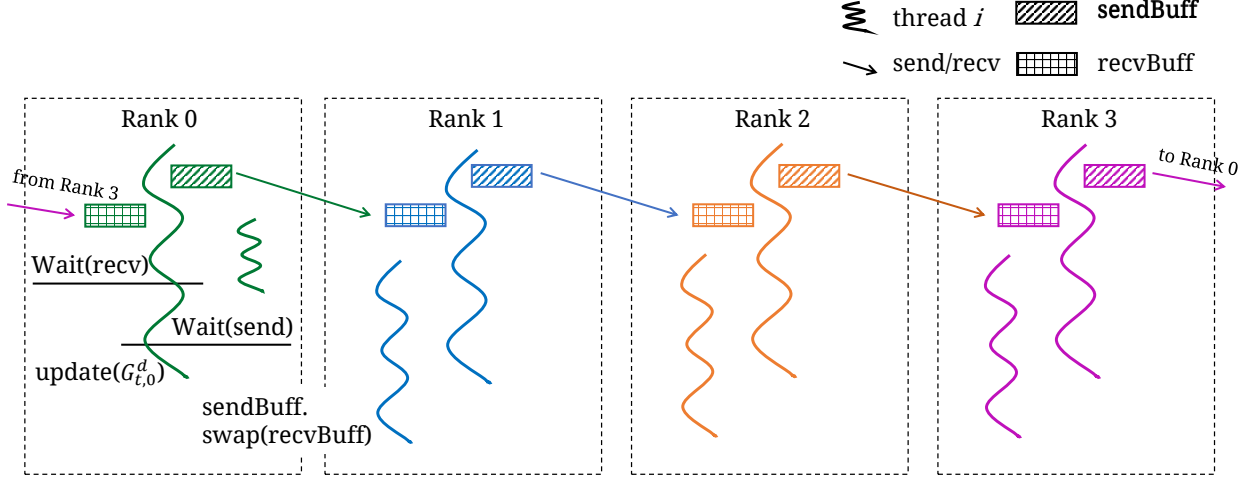


Figure 3: Workflow of ring algorithm per iteration.

At the start of every new measurement, a single-particle Green's function G_σ (Line 1) is generated and then used to update $G_{t,i}^d$ (Line 2) via the formula in Eq. (1). Between Lines 3 to 8, the algorithm initializes the indices of left and right neighbors and prepares the sending message buffer from the previously generated G_σ buffer. The processes are organized as a ring so that the first and last rank are considered to be neighbors to each other. A *swap* operation is used to avoid unnecessary memory copies for *sendBuff* preparation. A walker-accumulator thread allocates an additional *recvBuff* buffer of the same size as *gSigmaBuf* to hold incoming *gSigmaBuf* buffer from *leftRank*.

The *while* loop is the core part of the pipeline ring algorithm. For every iteration, each thread in a rank receives a G_σ buffer from its left neighbor rank and sends a G_σ buffer to its right neighbor rank. A synchronization step (Line 12) is performed afterward to ensure that each rank receives a new buffer to update the local $G_{t,i}^d$ (Line 13). Another synchronization step follows to ensure that all send requests are finalized (Line 14). Lastly, another *swap* operation is used to exchange content pointers between *sendBuff* and *recvBuff* to avoid unnecessary memory copy and prepare for the next iteration of communication. In the multi-threaded version (Section 3.2.2), the thread of index, i , only communicates with threads of index, i , in neighbor ranks, and each thread allocates two buffers: *sendBuff* and *recvBuff*.

The *while* loop will be terminated after $ringSize - 1$ steps. By that time, each locally generated $G_{\sigma,i}$ will have traveled across all MPI ranks and updated $G_{t,i}^d$ in all ranks. Eventually, each $G_{\sigma,i}$ reaches to the left neighbor of its birth rank. For example, $G_{\sigma,0}$ generated from rank 0 will end in last rank in the ring communicator.

Additionally, if the G_t is too large to be stored in one node, it is optional to accumulate all $G_{t,i}^d$ at the end of all measurements. Instead, a parallel write into the file system could be taken.

3.2.1 Sub-Ring Optimization.

A sub-ring optimization strategy is further proposed to reduce message communication times if the large device array G_t can fit in fewer devices. The sub-ring algorithm is visualized in Figure 4.

For the ring algorithm (Section 3.2), the size of the ring communicator ($mpiWorldSize$) is set to the same size of the global MPI_COMM_WORLD, and thus the size of G_t is equally distributed across all MPI ranks.

However, to complete the update to $G_{t,i}^d$ in one measurement, one $G_{\sigma,i}$ must travel $mpiWorldSize$ ranks. In total, there are $mpiWorldSize$ numbers of $G_{\sigma,i}$ being sent and received concurrently in one measurement in the global MPI_COMM_WORLD communicator. If the size of $G_{t,i}^d$ is relatively small per rank, then this will cause high communication overhead.

If G_t can be distributed and fitted in fewer devices, then a shorter travel distance is required for $G_{\sigma,i}$, thus reducing the communication overhead. One reduction step was performed at the end of all measurements to accumulate G_{t,s_i}^d , where s_i means i -th rank on the s -th sub-ring.

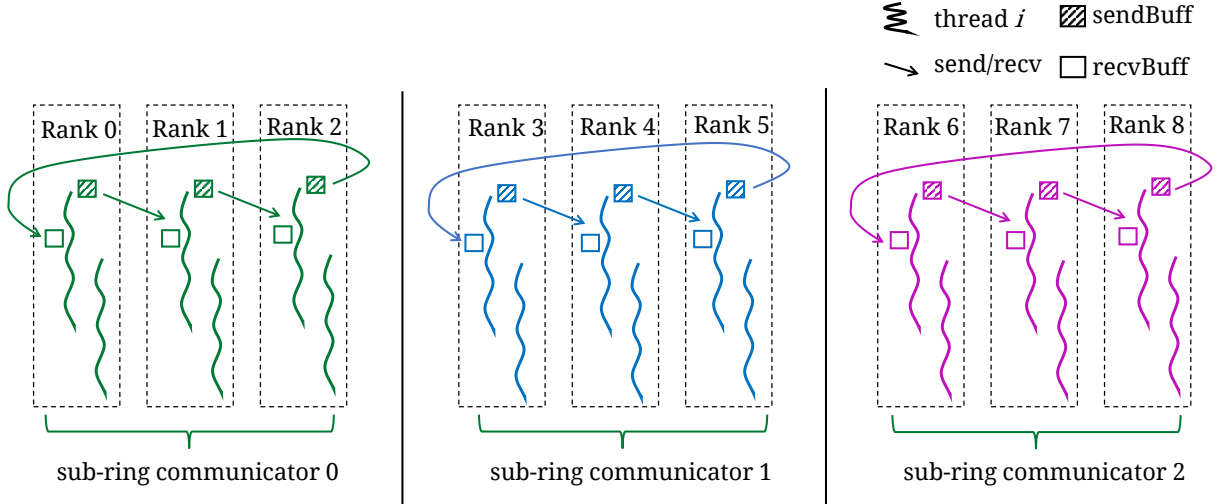


Figure 4: Workflow of sub-ring algorithm per iteration. Every consecutive S rank forms a sub-ring communicator, and no communication occurs between sub-ring communicators until all measurements are finished. Here, S is the number of ranks in a sub-ring.

At the beginning of MPI initialization, the global `MPI_COMM_WORLD` was partitioned into several new sub-ring communicators by using `MPI_Comm_split`. The new communicator information was passed to the DCA++ concurrency class by substituting the original global `MPI_COMM_WORLD` with this new communicator. Now, only a few minor modifications are needed to transform the ring algorithm (Algorithm 1) to sub-ring Algorithm 2. In Line 4, `myRank` is initialized to `subRingRank` instead of `worldRank`, where `subRingRank` is the rank index in the local sub-ring communicator. In Line 5, `ringSize` is initialized to `subRingSize` instead of `mpiWorldSize`, where `subRingSize` is the size of the new communicator. The general ring algorithm is a special case for the sub-ring algorithm because the `subRingSize` of the general ring algorithm is equal to `mpiWorldSize`, and there is only one sub-ring group throughout all MPI ranks.

Algorithm 2: Modified ring algorithm to support sub-ring communication

```
myRank ← subRingRank;
ringSize ← subRingSize;
```

3.2.2 Multi-Threaded Ring Communication.

To take advantage of the multi-threaded QMC model already in DCA++, multi-threaded ring communication support was further implemented in the ring algorithm. Figure 1 shows that in the original DCA++ method, each walker-accumulator thread in a rank is independent of each other, and all the threads in a rank synchronize only after all rank-local measurements are finished. Moreover, during every measurement, each walker-accumulator thread generates its own thread-private $G_{\sigma,i}$ to update G_t .

The multi-threaded ring algorithm now allows concurrent message exchange so that threads of same rank-local thread index exchange their thread-private $G_{\sigma,i}$. Conceptually, there are k parallel and independent rings, where k is number of threads per rank, because threads of the same local thread ID form a closed ring. For example, a thread of index 0 in rank 0 will send its G_{σ} to the thread of index 0 in rank 1 and receive another G_{σ} from thread index of 0 from last rank in the ring algorithm.

The only changes in the ring algorithm are offsetting the tag values (`recvTag` and `sendTag`) by the thread index value. For example, Lines 10 and 11 from Algorithm 1 are modified to Algorithm 3.

Algorithm 3: Modified ring algorithm to support multi-threaded ring

```
MPI_Irecv(recvBuf, source=leftRank, tag = recvTag + threadId, recvRequest);
MPI_Isend(sendBuf, source=rightRank, tag = sendTag + threadId, sendRequest);
```

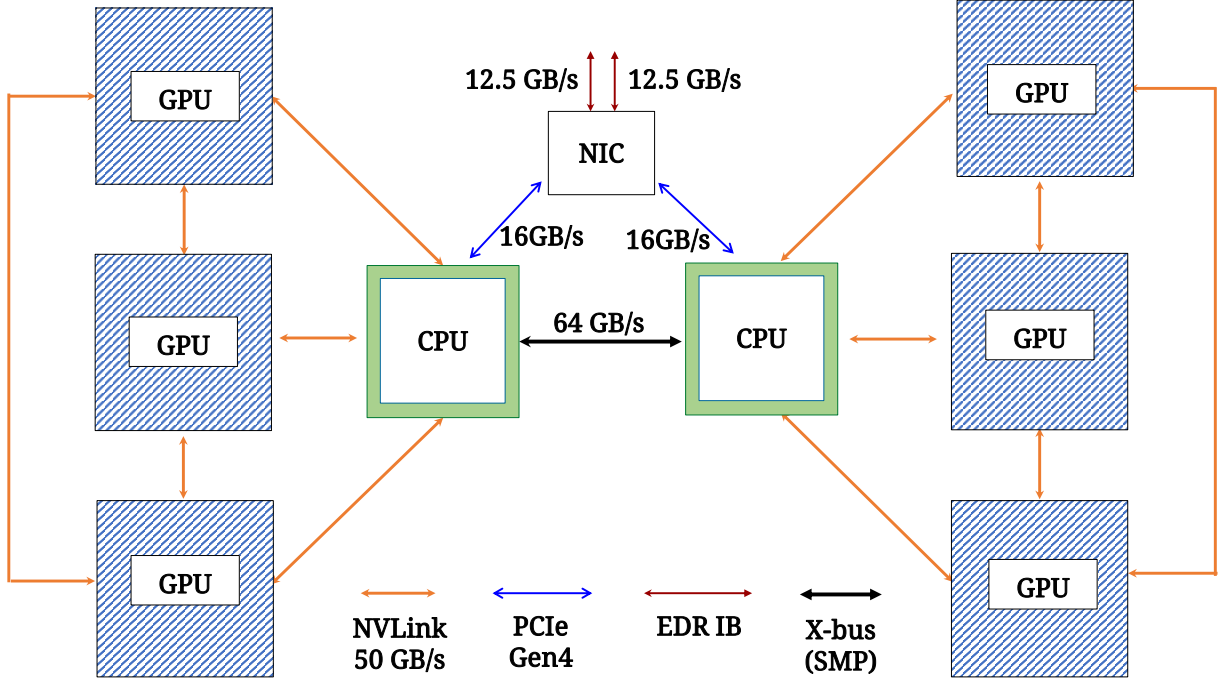


Figure 5: Architectural layout of a single node on Summit.

To efficiently send and receive G_σ , each thread will allocate one additional *recvBuff* to hold incoming *gSigmaBuf* buffer from *leftRank* and perform send/receive efficiently. In the original DCA++ method, there are k numbers of buffers of G_σ size per rank, and in the multi-threaded ring method, there are $2k$ numbers of buffers of G_σ size per rank, where k is number of threads per rank.

4 Results

This section evaluates this work from various perspectives—including correctness, memory analysis, scaling, and function activities—with help from the APEX profiling tool. All experiments were run on Summit.

4.1 Summit Node Configuration

Summit is a 4,600 node, 200 PFLOPS IBM AC922 system. Each node consists of two *IBM POWER9* CPUs with 512 GB DDR4 RAM and six NVIDIA V100 GPUs with a total of 96 GB high-bandwidth memory. Each Summit node (Figure 5) is divided into two sockets, and each socket has one *IBM POWER9* CPU and three NVIDIA V100 GPUs, all connected through NVIDIA’s high-speed NVLINK2. Each NVLINK2 is capable of a 25 GB/s transfer rate in each direction. Two *IBM POWER9* CPUs within a Summit node are connected through Peripheral Component Interconnect Express bus (64 GB/s bidirectional). There is a Mellanox Infiniband EDR network interface connector (NIC) attached to each Summit node (two ports per NIC, 12.5 GB/s per port).

4.2 APEX

APEX [6] is a performance measurement library for distributed, asynchronous multitasking systems. It provides lightweight measurements without perturbing high concurrency through synchronous and asynchronous interfaces. To support performance measurement in systems that employ operating system- or user-level threading, APEX uses a dependency chain in addition to the call stack to produce traces and task dependency graphs. The synchronous APEX instrumentation application programming interface (API) can be used to add instrumentation to a given run time and includes support for timers and counters. To support C++ threads on Linux systems, the underlying POSIX threads are automatically instrumented by using a preloaded shared object library that intercepts and wraps pthread calls in the application. The NVIDIA CUDA Profiling Tools Interface [7] provides CUDA host callback and device activity measurements. Additionally, the hardware and operating system are monitored through an asynchronous

Table 1: Comparison of function differences between the original G_t and accumulated G_t^d over five runs.

Error	Real part	Imaginary part	<5e-7
L1	3.71e-09±1.74e-18	4.61e-09±2.16e-18	True
L2	3.10e-10±4.19e-18	3.37e-10±3.89e-18	True

measurement that involves the periodic or on-demand interrogation of the operating system, hardware states, or run time states (e.g., CPU use, resident set size, memory “high water mark”). The NVIDIA Management Library interface [8] provides periodic CUDA device monitoring to APEX. For this work, APEX was extended to capture additional timers and counters related to CUDA device-to-device memory transfers, and support for key MPI calls was provided by a minimal implementation of the MPI Profiling Interface [9].

4.3 Accuracy Analysis

To verify that this implementation generates correct results, the same input configuration was run for original and ring algorithm methods, and the differences between the original G_t and accumulated G_t^d arrays were compared. A normalized L1 loss function (least absolute deviations, Eq. [2]) and normalized L2 loss function (least square errors, Eq. [3]) were used to compute the normalized error between original G_t and accumulated G_t^d arrays in which the “entrywise” norm was used.⁵ The baseline is that the $L1_error$ and $L2_error$ between two arrays should be smaller than 5e-7 after DCA++ testing protocol, where:

$$L1_error = \frac{\|\text{vec}(G_t - G_t^d)\|_1}{\|\text{vec}(G_t)\|_1}, \quad (2)$$

$$L2_error = \frac{\|\text{vec}(G_t - G_t^d)\|_2}{\|\text{vec}(G_t)\|_2}. \quad (3)$$

For input configuration, the single-band Hubbard model was chosen because it is a standard model of correlated electron systems and is used in almost all the studies of the cuprate high-temperature superconductors. Moreover, the cluster size was configured to 36-site (6x6 cluster), which is state-of-the-art simulations size. 100,000 Monte Carlo measurements were chosen to observe runtime performance of the ring algorithms as the runtime scales linearly with the number of measurements for constant number of ranks. Since the cluster size was configured to 6*6 and four-point-fermionic-frequencies was set to 64, this leads 212,336,640 entries in G_t . Since each G_t entry is a double-precision complex number, the G_t memory size is about 3.4 GB. This configuration can produce large G_t but still will not hit memory-bound issues on Summit GPUs—in which each GPU has 16 GB—for the regular G_t version. Such configurations were run on one Summit node five times with six ranks per node and seven walker-accumulator threads per rank. For the distributed G_t^d version, ring size was set to six so there was only one sub-ring during the run. The results show that the implementation generates correct results (Table 1) because the $L1_error$ and $L2_error$ on accumulated G_t^d are in an acceptable range.

4.4 Memory Analysis

The memory analysis results show that device memory required for G_t^d decreases linearly to the size of the sub-ring or the number of MPI ranks in the sub-communicator, which fits the ring algorithm. The APEX profiling tool was used to collect memory allocation information over the time. The performance results reflect correctly to the ring algorithm method because the G_t was evenly distributed across MPI ranks—in which each rank uses 1 GPU—within one sub-ring communicator.

For example, the requested size in `cudaMalloc` API was compared between original G_t (Figure 6a) and distributed G_t^d (sub-ring size of three, Figure 6b) methods. This shows that the distributed G_t^d method produced three times less memory allocation than the original G_t device array. At around 7 s in both cases, the distributed G_t^d method allocated 1.13 GB for $G_{t,i}^d$, and the original G_t method allocated 3.40 GB for $G_{t,i}$.

⁵Entrywise norm as defined in https://en.wikipedia.org/wiki/Matrix_norm

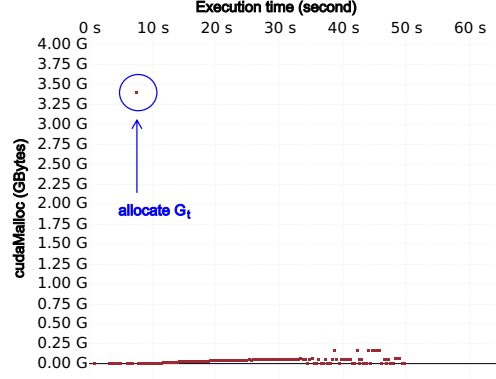
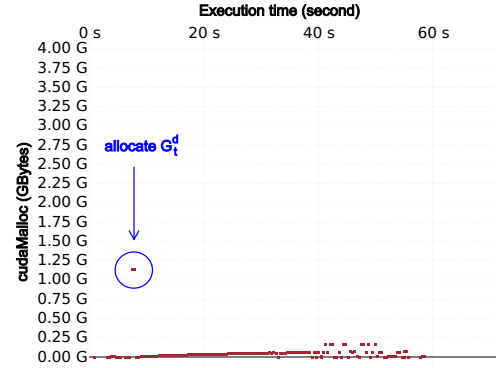
(a) Original G_t implementation.(b) Distributed G_t^d implementation with sub-ring size of three.

Figure 6: cudaMalloc requested size (GB) over time visualized by Vampir.

4.5 Scaling Results

In the pipeline sub-ring algorithm, each rank sends $S - 1$ and receives $S - 1$ messages, where S is the size of sub-ring. Thus, the total number of messages scales quadratically as $O(S^2)$, but the number of messages crossing each communication link increases linearly as $O(S)$. Figure 7 shows the elapsed computation time for 1,400 measurements (per rank) of the sub-ring algorithm running with six ranks per Summit node in which each message is about 170 MB. The data are well approximated by a linear least-square line that indicates that the elapsed computation time increases linearly as the sub-ring size increases. This suggests that the sub-ring algorithm is not constrained by the total volume of messages but is restricted by the slowest communication link. The effective bandwidth of the sub-ring algorithm can be estimated as:

$$\text{effective bandwidth} \approx (170 * 10^6 * S * 1,400) / (\text{elapsed time}),$$

and this is about 6 GB/s using the data for $S = 60$ on 10 nodes in Figure 7. This effective bandwidth is about 50% of the theoretical peak bandwidth for the NIC (12.5 GB/s per port) on the Summit node.

The authors acknowledge that enabling the ring algorithm to solve existing small problem-size (single band hubbard model with lower cluster size) will be an overkill, since the communication overhead will drastically increase the runtime; therefore the authors propose, the ring algorithm be only used when the G_t cannot fit into one single GPU memory. When the original DCA++ is executed with a large enough problem size (when G_t cannot fit into one single GPU), the program simply crashes failing to allocate memory on the device. Moreover, The scalability issue of the ring algorithm was the core focus for the authors during the implementation and the optimization design strategies of the sub-ring algorithm. Without sub-ring optimization, the originally proposed ring algorithm will potentially take undesirably long period of time to finish a run of DCA++, especially when requesting thousands of compute nodes. With the sub-ring optimization, scientists are able to run large science cases while maintaining acceptable communication overhead.

Since the current sub-ring size has to be configured manually, the authors plan to design a runtime adaptivity optimization that will automatically adapt the optimal sub-ring size. This optimization will distribute G_t into the minimal number of devices as well as preserves optimal runtime performance. This runtime adaptivity will be very

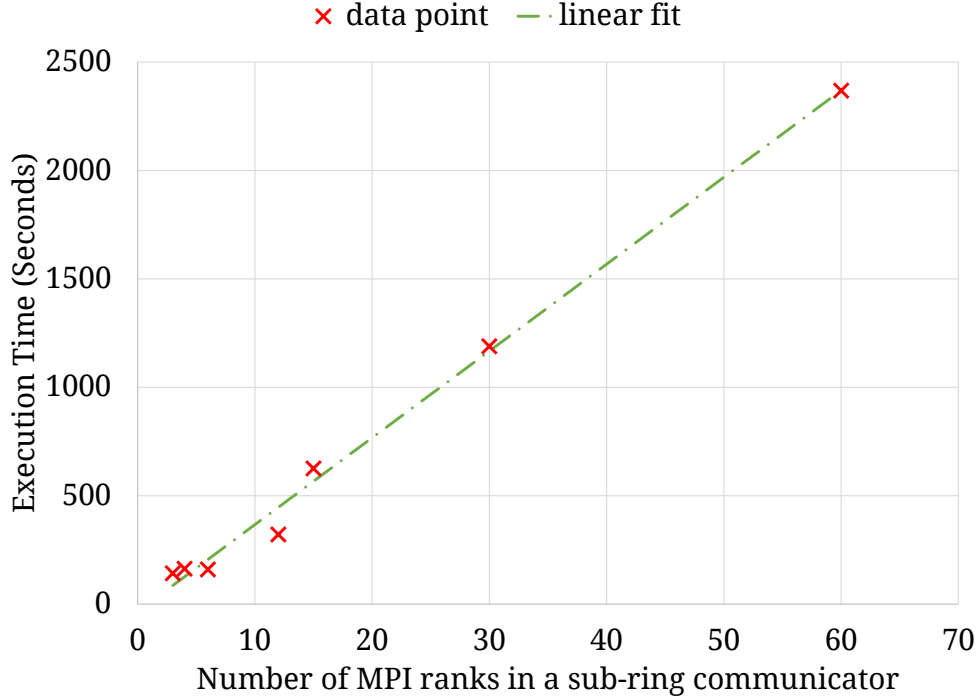


Figure 7: Time for 1,400 iterations (per rank) of the sub-ring algorithm using six ranks per Summit node, and each message size is 170 MB.

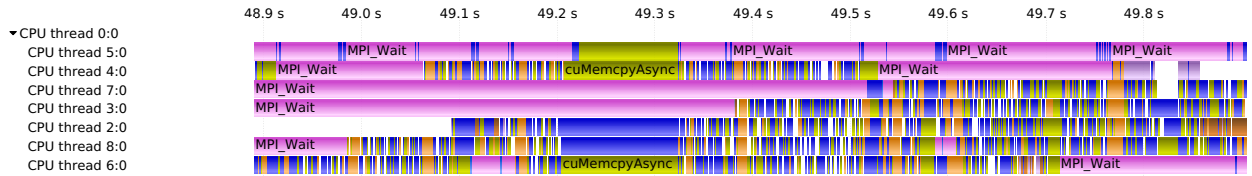


Figure 8: Vampir timeline graph shows the processes’ activities over the time in rank 0 (DCA++ with multi-threaded ring algorithm).

helpful because DCA++ is an iterative convergence algorithm and thus G_t size could be dynamically changed over multiple DCA++ runs for production science runs on leadership computing facilities.

5 Discussion

5.1 Concurrency Overlapping

The multi-threaded ring implementation provides sufficient concurrency that overlaps communication and computation. The APEX profiling tool was used to collect data on process activities over time and visualize the data in Vampir.

DCA++ was run with multi-threaded ring support and obtained the timeline activities in rank 0 at 49 s (Figure 8). Some concurrency overlap was observed in the multi-threaded ring algorithm so that although some threads are blocked in `MPI_Wait`, other threads of the same rank perform useful computation tasks. For example, the short blocks that are not labeled as `MPI_Wait` are mostly related to kernel activities.

The current ring algorithm was also observed to be a lock-step algorithm in which the next computation (update G_t) cannot start until the previous communication step (G_σ message exchange) is finished. To expose more concurrency, HPX [10]—a task-based programming model—could be used to overlap the communication and computation. For example, DCA++ kernel function can be wrapped into an HPX *future*, which represents an ongoing computation and asynchronous task. Then, the communication tasks can be attached or chained to the “futurized” kernel task. Wei et

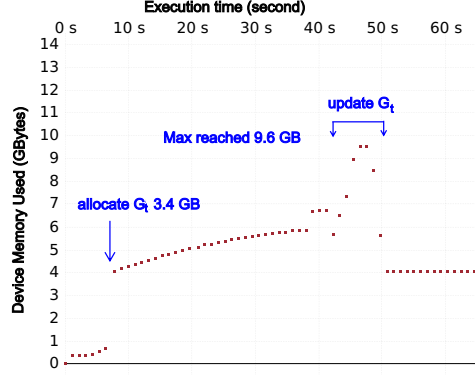
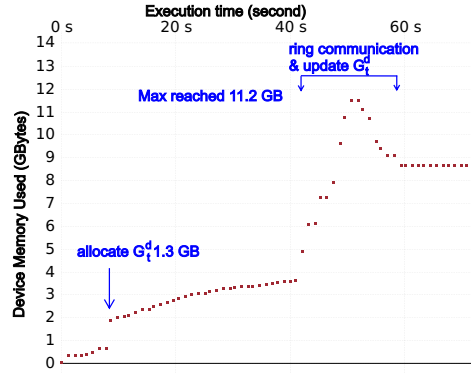
(a) Original G_t method.(b) Distributed G_t^d method with sub-ring size of three.

Figure 9: Device memory used (GB over time) when using seven walker-accumulator thread. Visualized by Vampir.

al. [4] reported that DCA++ with HPX user-level [11] threading support achieves a 20% speedup over the original C++ threading (kernel-level) due to faster context switching in HPX threading.

5.2 Trade-Off between Concurrency and Memory

As walker-accumulator threads increase in the multi-threaded ring algorithm, GPU memory usage is also increased because more device memory is needed to store extra thread-private $G_{\sigma,i}$ buffers. This might cause a new memory-bound challenge if too many concurrent threads are used. One possible solution is to reduce concurrent threads to achieve more usable device memory.

The same configuration was run for the original G_t and distributed G_t^d versions with seven threads and then with one thread, respectively (Figure 9).

For the comparison on seven threads (Figures 9a and 9b), the first spike in memory usage increase is due to G_t allocation, and the second significant wave is because each thread is allocating $G_{\sigma,i}$.

The original algorithm needs 3.4GB for G_t and 9.6GB in total, and the new algorithm needs 1.3GB for G_t^d and 11.2 GB in total. The non- G_t allocation in the original algorithm is 6.2 GB, and distributed G_t^d method is 9.9GB, which leads to the overhead of 3.7 GB in G_t^d version. The $G_{\sigma,i}$ is composed of two same-size matrices (spin up and spin down matrix, each matrix is sized at 0.17 GB). In the original algorithm, the total G_{σ} allocation is $0.17 \times 2 \times 7 = 2.38$ GB where 2 is the two matrices (up and down) in $G_{\sigma,i}$ and 7 is seven threads. In the distributed G_t^d method, the total G_{σ} allocation is $0.17 \times 2 \times 3 \times 7 = 7.14$ GB where 3 is three allocations ($G_{\sigma,i}$ itself, $sendBuf$, $recvBuf$) per thread. The overhead of overall G_{σ} allocation in the ring algorithm is $7.14 - 2.38 = 4.76$ GB, which is about 1 GB more than the non- G_t allocation (3.7GB). In Figure 9a, there is a significant reduction of allocated memory in the 42nd second, which is 1GB memory deallocation in G_{σ} . However, we did not observe a similar drop or wave pattern in Figure 9b because those $sendBuf$, $recvBuf$ matrices are not dynamically allocated so that the dip before the allocations was hidden. This explains the 1GB difference.

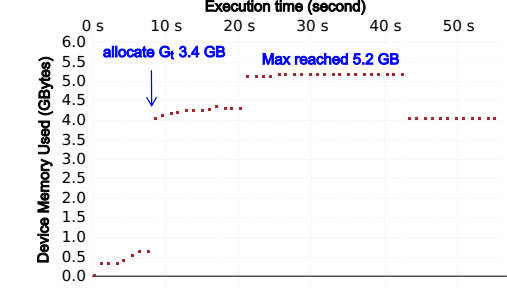
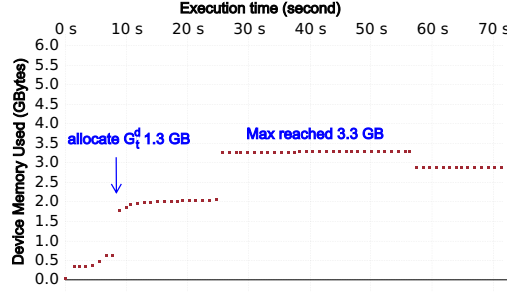
(a) Original G_t method.(b) Distributed G_t^d method with sub-ring size of three.

Figure 10: Device memory used (GB over time) when using one walker-accumulator thread. Visualized by Vampir.

However, if only one thread was used (Figures 10a and 10b), then the maximum device usage in the distributed G_t^d version (3.3 GB) is 1.9 GB less than the one in the original G_t version (5.2 GB). Much more usable device memory can be gained if concurrent walker-accumulator threads are reduced. For example, the saved device memory from reduced threads can be used to fit larger G_t . Furthermore, a comparison experiment was run on one Summit node (six ranks per node) by using the same input configuration (sub-ring size is three, measurement is 4,200 total), except for threading numbers per rank. The distributed G_t^d with seven threads (87 s) has 1.3 times more speedup than the one with one thread (116 s). This result suggests that if there is insufficient device memory, then the code might use fewer threads with some loss (less than 30%) of run time performance. The authors are considering quantifying and modeling this trade-off in their future research development.

To solve the NIC bottleneck issue and the new memory-bound challenge caused by multi-threaded communication (storing additional G_σ), the authors are considering another plan to move G_σ to the CPU host in which the CPU host has more memory. Each Summit node contains 512 GB of DDR4 memory for use by the *IBM POWER9* processors,⁶ and there are only $6 * 16 \text{ GB} = 96 \text{ GB}$ of device memory. On Summit, the NICs are connected to the CPU and are not directly connected to the GPU. The NVLINK2 connection between CPU and GPU has peak of 50 GB/s, so it is faster compared with NIC's peak bandwidth (12.5 GB/s) and might not be the bottleneck. One possible future extension could be to consider keeping G_t on the CPU side instead of in GPU device memory so that a smaller sub-ring can be used or so the sub-ring can be kept on the same single node.

Additionally, the authors have explored bidirectional ring implementation that alternates ring communication directions between threads. After extensive testing, the authors concluded that the bidirectional ring improved performance up to 1.3X across-rack (each rack has 18 compute nodes on Summit) over the current unidirectional ring. However, there are no potential performance benefits using the bidirectional ring approach over the current unidirectional ring when reserving the whole rack. Authors continue to investigate in coordination with hardware vendors to address the performance of bidirectional ring implementation.

6 Conclusions

This paper presents how the authors successfully solved the memory-bound challenge in DCA++, which will allow physicists to explore significantly large science cases and increase the accuracy and fidelity of simulations of certain materials. An effective “all-to-all” communication method—a ring abstraction layer—was designed for this purpose so

⁶Summit User Guide: https://docs.olcf.ornl.gov/systems/summit_user_guide.html

that the distributed device array G_t can be updated across multi-GPUs. The G_t device array was distributed across multi-GPUs so that the allocation size for the most memory-intensive data structure per GPU is now reduced to $1/p$ of the original size, where p is number of GPUs in the ring communicator. This significant memory reduction (much larger G_t capability) is the primary contribution from this work because condensed matter scientists are now able to explore much larger science cases.

In calculating the full 4-point correlation function G_t , the storage of G_t grows as $O(L^3 F^3)$ where L is the number of cluster sites and F is the number of frequencies. This new capability will enable large-scale simulations such as 36-site (6x6 cluster) with over 64 frequencies to (1) obtain more accurate information, and (2) enable resolution of longer wavelength correlations that have longer periodicity in real space and which cannot be resolved in smaller clusters. The system size can grow fairly large and depends on how much memory the leadership computing facilities can provide. Relevant science problems that the domain specialists would like to study range in the orders of 10s-of-100s of Gigabits of G_t , potentially opening up more research into how we can use the host memory without losing performance.

The ring algorithm implementation takes advantage of GPUDirect RDMA technology, which can directly and efficiently exchange device memory. Several optimization techniques were used to improve the ring algorithm performance, such as sub-ring communicators and multi-threaded supports. These optimizations reduced communication overhead and expose more concurrency, respectively. Performance profiling tools were also improved, such as APEX, which now allows more kernel and communication information to be captured in-depth. The ring algorithm was demonstrated to effectively reduce the memory allocation needed for the G_t device array per GPU. This paper also discusses various trade-offs between concurrency and memory usage for the multi-threaded ring algorithm and the NIC bottleneck issue. In the future, the authors plan to explore the HPX run time system to overlap the computation and communication in DCA++ to expose more concurrency and asynchronicity.

Acknowledgement

Authors would like to thank Thomas Maier (ORNL), Giovanni Balduzzi (ETH Zurich) for their insights during the optimization phase of DCA++.

This work was supported by the Scientific Discovery through Advanced Computing (SciDAC) program funded by U.S. Department of Energy, Office of Science, Advanced Scientific Computing Research (ASCR) and Basic Energy Sciences (BES) Division of Materials Sciences and Engineering, as well as the RAPIDS SciDAC Institute for Computer Science and Data under subcontract 4000159855 from ORNL. This research used resources of the Oak Ridge Leadership Computing Facility, which is a DOE Office of Science User Facility supported under Contract DE-AC05-00OR22725, and Center for Computation & Technology at Louisiana State University.

References

- [1] M. H. Hettler, A. N. Tahvildar-Zadeh, M. Jarrell, T. Pruschke, and H. R. Krishnamurthy. Nonlocal dynamical correlations of strongly interacting electron systems. *Phys. Rev. B*, 58:R7475–R7479, Sep 1998.
- [2] M. H. Hettler, M. Mukherjee, M. Jarrell, and H. R. Krishnamurthy. Dynamical cluster approximation: Nonlocal dynamics of correlated electron systems. *Phys. Rev. B*, 61:12739–12756, May 2000.
- [3] Thomas Maier, Mark Jarrell, Thomas Pruschke, and Matthias H. Hettler. Quantum cluster theories. *Rev. Mod. Phys.*, 77:1027–1080, Oct 2005.
- [4] Weile Wei, Arghya Chatterjee, Kevin Huck, Oscar Hernandez, and Hartmut Kaiser. Performance analysis of a quantum monte carlo application on multiple hardware architectures using the hpx runtime. 2020.
- [5] Giovanni Balduzzi, Arghya Chatterjee, Ying Wai Li, Peter W Doak, Urs Haehner, Ed F D’Azevedo, Thomas A Maier, and Thomas Schulthess. Accelerating DCA++ (dynamical cluster approximation) scientific application on the Summit supercomputer. In *2019 28th International Conference on Parallel Architectures and Compilation Techniques (PACT)*, pages 433–444, Seattle, WA, USA, 2019. IEEE.
- [6] Kevin A Huck, Allan Porterfield, Nick Chaimov, Hartmut Kaiser, Allen D Malony, Thomas Sterling, and Rob Fowler. An autonomic performance environment for exascale. *Supercomputing frontiers and innovations*, 2(3):49–66, 2015.
- [7] NVIDIA. Cuda profiling tools interface, 2020. <https://docs.nvidia.com/cuda/cupti/index.html>.

- [8] NVIDIA. Nvidia management library (nvml), 2020. <https://developer.nvidia.com/nvidia-management-library-nvml>.
- [9] Marc Snir, Steve Otto, Steven Huss-Lederman, David Walker, and Jack Dongarra. *MPI: The Complete Reference*. The MIT Press, Cambridge, MA, USA, 1998.
- [10] Hartmut Kaiser, Patrick Diehl, Adrian S. Lemoine, Bryce Adelstein Lelbach, Parsa Amini, Agustín Berge, John Biddiscombe, Steven R. Brandt, Nikunj Gupta, Thomas Heller, Kevin Huck, Zahra Khatami, Alireza Kheirkhahan, Auriane Reverdell, Shahrzad Shirzad, Mikael Simberg, Bibek Wagle, Weile Wei, and Tianyi Zhang. HPX - the C++ standard library for parallelism and concurrency. *Journal of Open Source Software*, 5(53):2352, 2020.
- [11] Tianyi Zhang, Shahrzad Shirzad, Patrick Diehl, R Tohid, Weile Wei, and Hartmut Kaiser. An introduction to hpxMP: A modern OpenMP implementation leveraging HPX, an asynchronous many-task system. In *Proceedings of the International Workshop on OpenCL*, pages 1–10, New York, NY, United States, May 2019. Association for Computing Machinery.